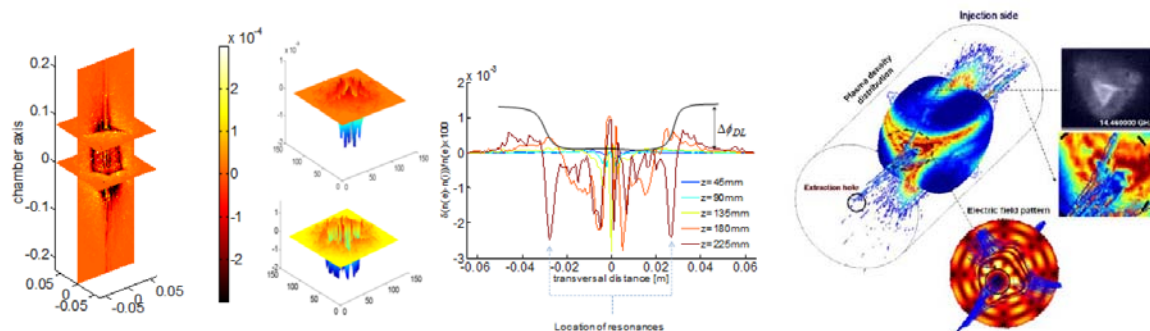


## Report on experimental results of microwave to plasma coupling and description of the ion sources improvements obtained in the frame of the JRA

### 1. Plasma and electromagnetic field simulations: results and achievements (LNS, ATOMKI, GSI )

Very promising results have been achieved from the simulations carried out from INFN-LNS ion source group. Such calculation highlight a strong influence of plasma heating peculiarities not only on the electron dynamics (heating rapidity, confinement properties) but also on the ion dynamics, which are mostly governed by: 1) strong non-homogeneous distribution of the plasma density inside the chamber (formation of the high density plasmoid); 2) generation of a double layer at the resonance surface, which consequently leads to a radial self-developed potential dip; 3) remarkable depletion of the plasma density in the near axis zone, as a consequence of weak RF contribution to inner plasmoid electron confinement. Figure 1 synthetically reassumes the modelling results, and shows the formation of the radial potential dip which confines the highly charged ions pushing them in near axis zone.



**Figure 1** - (left) 3D view of DL in correspondence of ECR layer; (center) 1D trend of the density fluctuations along different transversal axes, and expected profile of the DL potential. 3D electron density and pattern of electromagnetic field compared with the real shape of the extracted ion beam.

The simulation strategy has been further upgraded by introducing self-consistency: the method consists in a strict interplay between COMSOL (solving Maxwell equations) and MATLAB (for the particles kinetics). The new approach shows that although the vacuum field RF field distribution is perturbed by the plasma medium, the non-uniformity in the electric field amplitude still persists in the plasma filled cavity.

According to simulation results, hence, it seems the variations in the beam shape are caused by different structures of the plasma under different pumping wave frequencies. The common feature of hollow beams could be indeed due to the plasma density depletion in near axis zone, caused by the typical low electric field amplitude available in that region for high order modes excited into the plasma chamber (see figure 1-right). Some plasma features are now clear according to pictures of figure 2: i) the plasma concentrate mostly in near resonance region: a dense plasmoid is surrounded by a rarefied halo; ii) at different energies distribute differently in the space: cold electrons in the core, hot ones in near ECR regions; iii) ions are formed where hot electrons are placed; iv) this implies the ion beam shape depends on

electron/ion distribution on the plasmoid surface. Therefore, optimization of the ion beam formation must begin well inside the plasma.

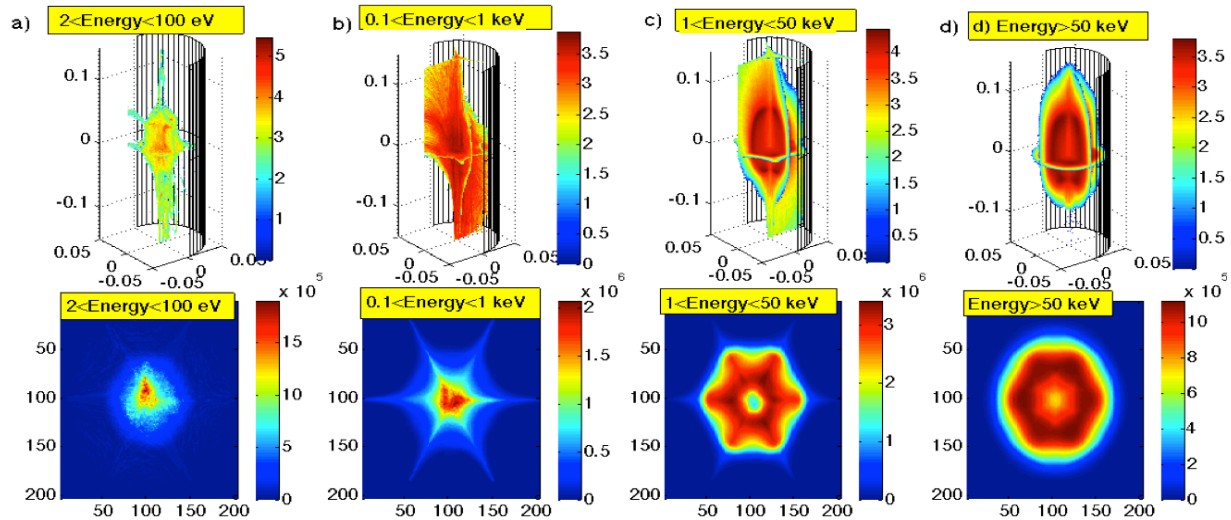


**Figure 2:** Upper row: 3D density distribution [a.u] at different energy ranges (a.u. in log scale); Lower row: integrated density distribution in a 2D transversal view (a.u. in linear scale).

The ATOMKI ECR team calculated the spatial and energy structure of the non-lost (plasma) electrons in the 14 GHz ATOMKI-ECRIS by using the TrapCAD simulation code. 3 million electrons were placed with equal density into a thin layer developed by the closed resonance zone (RZ). The simulation time was 200 nanoseconds, in real (CPU) time the calculation lasted for 127 hours. At the end of the simulation 49% (1.46 million) of the electrons were still remained in the plasma and 51% lost on the chamber wall. The average energy of the non-lost electrons increased from 100 eV up to 3330 eV by the ECR heating process. The non-lost electrons were filtered by their energies ( $E < 200 \text{ eV}$ : cold electrons,  $200 \text{ eV} < E < 3 \text{ KeV}$ : intermediate electrons,  $3 \text{ KeV} < E < 10 \text{ KeV}$ : warm electrons,  $E > 10 \text{ KeV}$ : hot electrons). The electron density distribution along the plasma chamber axes demonstrates the significant difference between the electron populations (see figure 3). Cold electrons are found all along the plasma chamber – according to the many visual observations (cold electrons excite atoms which emit visible light photons).

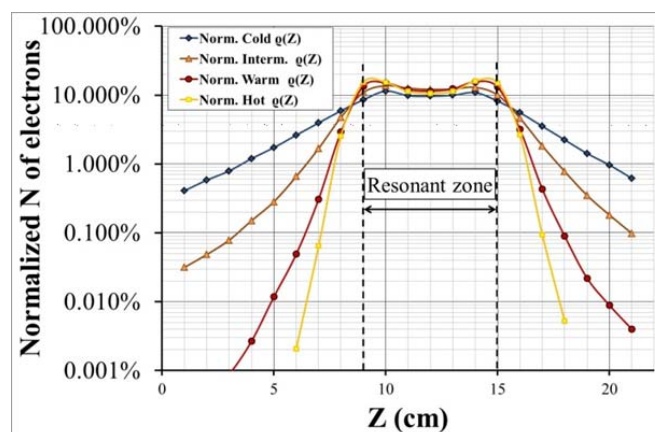


**Figure 3:** Normalized electron density distributions along the plasma chamber axes

The warm (ionizing) electrons concentrate much more around the resonance zone (RZ). They are two order of magnitude less near the chamber end-plates ( $z=1$  and  $z=20$ ) than the cold electrons. The density of the hot electrons outside the RZ is more than 3 orders of magnitude less than near the RZ. For all energy components the general conclusion is that the electrons separate into a high density inner plasma (developed by the RZ) surrounded by a lower density halo. A comparison was made between the simulations and the photos of plasma made from He, methane, N, O, Ne, Ar, Kr, Xe gases and from their mixtures taken at ATOMKI ECRIS and consequences were withdrawn to the cold electron component of the plasma. The warm electron component of the simulation was compared with X-ray photos emitted by plasma ions (see figure 4). The results and information significantly improve the understanding of the ECRIS plasma and may help the work of ion source and extraction optics designers.

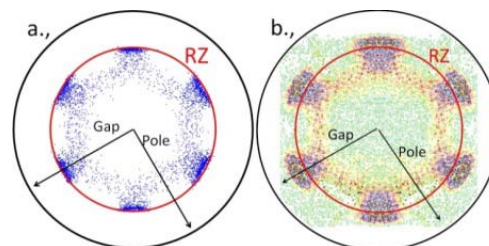


**Figure 4:** Computer simulation of the warm electron cloud of a 14.3 GHz plasma (left). The X-ray photo (right) shows the spatial positions of the ions in the same plasma

The software CST Microwave Studio was used at GSI to simulate the electromagnetic field excited inside the plasma chamber, including the copper cube and the plasma electrode, of the CAPRICE ECRIS, and the results are shown in figure 5.

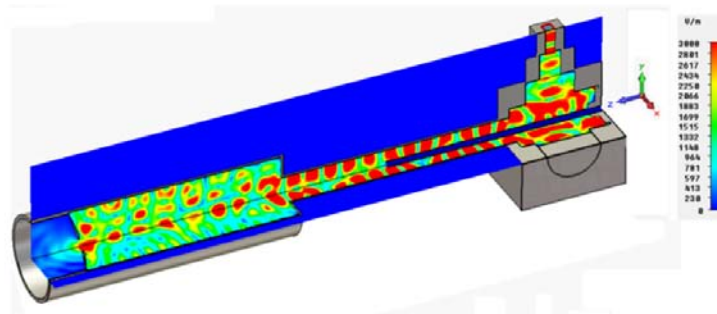


**Figure 5:** Electric field amplitude at 14.5 GHz for the yz and zx planes relative to the upper right part of the structure

## 2. Experiments results on plasma coupling (JYFL,LNS, GSI)

A network analyzer based measurement setup was used at University of Jyvaskyla to study the resonance properties of plasma filled electron cyclotron resonance ion source (ECRIS) plasma chamber. The loaded cavity measurements were performed using a dual port technique, in which two separate waveguides were used simultaneously (see figure 6). One port was used to ignite and sustain the plasma with a microwave source operating around 11 GHz and the other was used to probe the cavity properties with the network analyzer using a frequency range around 14 GHz. Figure 7 shows the behavior of  $S_{11}$  parameter ( $S_{11} = 10\log_{10}(P_{\text{refl}}/P_{\text{fwd}})$ ) as a function of probing and not-perturbing frequency. The parameter describes the ability of system to absorb the microwave

power at certain frequency. The main plasma was maintained with the TWTA and its output power was altered as indicated by the figure 7. The left-hand side graph shows the effect of power on the mode behavior. The uppermost part shows the behavior of  $S_{11}$  parameter without the plasma, i.e. in this case the power from TWTA was switched OFF. As graph shows, the variations in  $S_{11}$  parameter decrease when the microwave power was increased. This indicates that the plasma density increases and consequently most of the power is absorbed by the plasma resulting in broader and shallower minima of  $S_{11}$  parameter. The right-hand side graph shows that the exact resonance frequency of the (arbitrarily selected) mode moves towards higher frequencies as a function of plasma density, i.e. when the microwave power increases.

A similar experiment was carried out at GSI in collaboration with LNS to validate and to measure the standing wave presence in an ECR plasma.

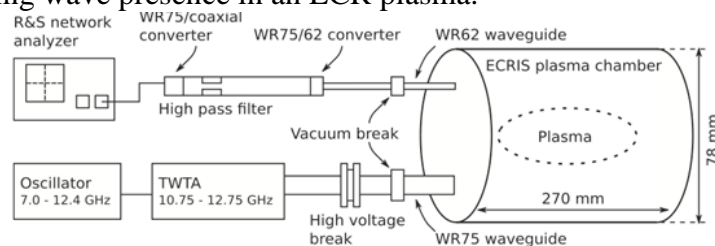


**Figure 6:** Setup for the dual port coupling measurement of plasma loaded cavity

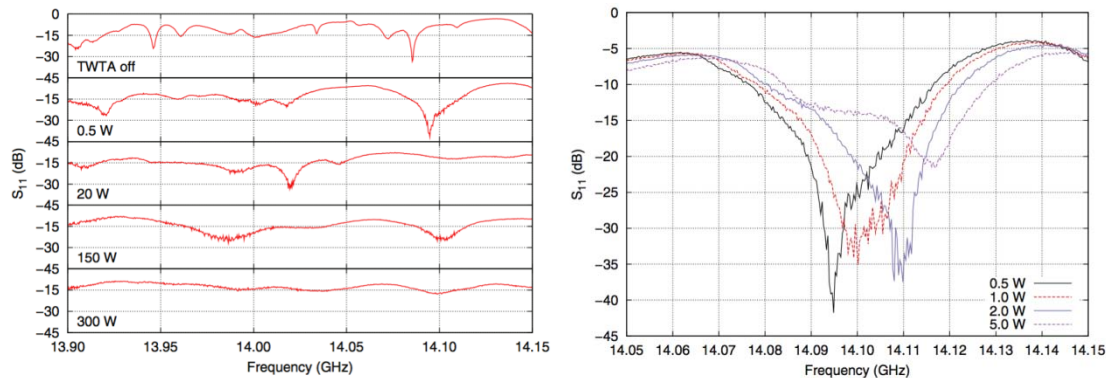


**Figure 7:** The effect of the microwave power on the mode behavior.

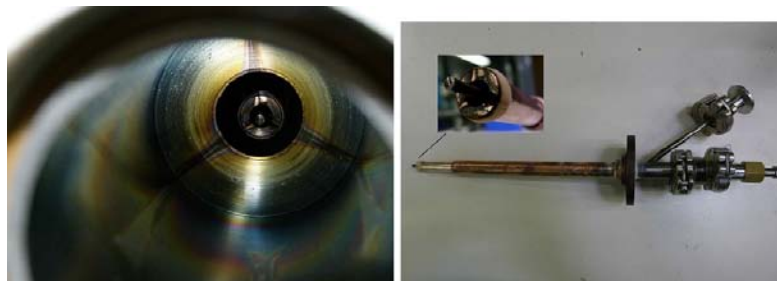


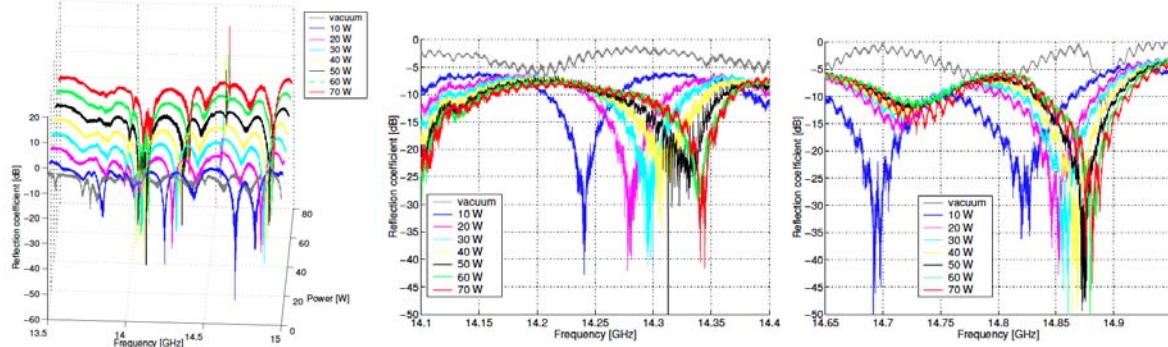
**Figure 8:** Coaxial probe inserted into the oven housing (right) and view of the internal tip inside the plasma chamber (left).

In order to measure the reflection coefficient with and without the plasma a coaxial probe was guided inside the CAPRICE ECRIS into the oven housing up to the end of the first section of the plasma chamber where a tip was inserted (see figure 8). A Traveling Wave Tube Amplifier driven by a synthesizer was used to create the plasma, made with He and Ar, with a

power increasing up to 70 W at steps of 10 W. During the plasma creation the reflection coefficient was measured in the 13.5-15 GHz frequency range with the Network Analyzer connected to the coaxial probe. Results are shown in the set of figures 9. The frequency feeding the plasma was clearly coupled to the coaxial probe and resonances measured in vacuum conditions shifted toward higher values with the power as observed at JYFL.

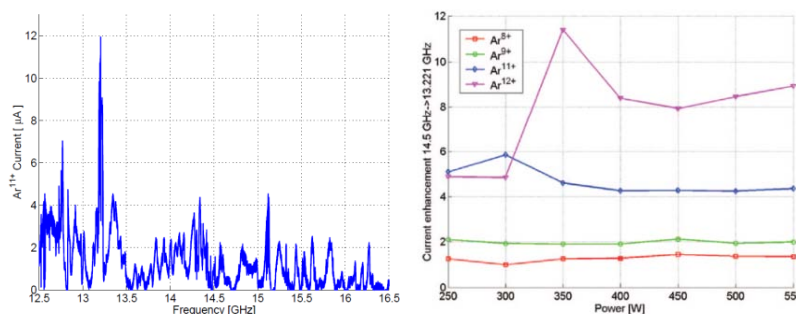
### 3. Frequency tuning measurements (GSI,LNS,IKF,IFIN-HH)

The frequency tuning technique, based on the variation of the microwave frequency feeding the ECR plasma, has been experimentally investigated with the CAPRICE-type ECRIS installed in the ECR injector test setup (EIS) of GSI, in collaboration with the INFN-LNS ion source group. The experimental setup comprised a Travelling Wave Tube Amplifier (TWTA) driven by a signal generator and connected to the ion source through a WR62 rectangular waveguide. The ECRIS parameters were set in order to maximize the production of the  $\text{Ar}^{11+}$



**Figure 9:** (left) Reflection coefficient measured at the coaxial probe when the plasma is created at the waveguide input for different microwave powers and detailed view in the ranges 14.1-14.4 GHz (center) and 14.65-14.95 GHz (right).

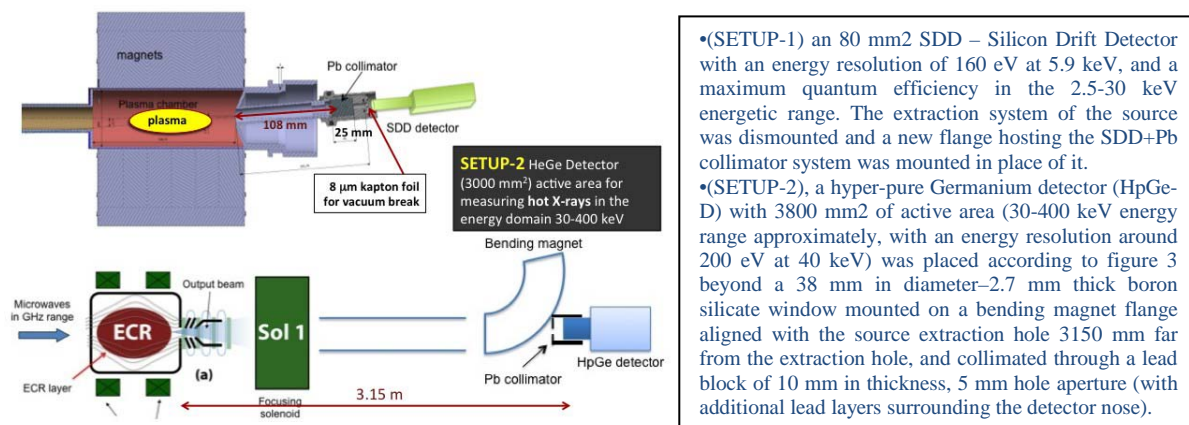
ion current. Then frequency sweeps in the 12.5-16.5 GHz frequency range (at a microwave power of 450 W) were performed while measuring the  $\text{Ar}^{11+}$  current. The result is shown in the figure 10-left. Some frequencies can be identified at which the  $\text{Ar}^{11+}$  current is considerably enhanced with respect to the standard operating frequency of 14.5 GHz. The charge state distributions were measured at different values of microwave power varied between 250 W and 550 W in steps of 50 W for two microwave frequencies: 14.500 GHz and 13.221 GHz, where the maximum of the  $\text{Ar}^{11+}$  intensity appears, respectively. All other ion source parameters were kept constant. As result the right figure 10 shows the ratio of the  $\text{Ar}^{q+}$  ( $q = 8, 9, 11, 12$ ) currents corresponding to the two frequencies as function of the microwave power.



**Figure 10:**  $\text{Ar}^{11+}$  current measured as function of the microwave frequency (left) and current enhancement for different microwave powers when the frequency is shifted from 14.500 GHz to 13.221 GHz (right).

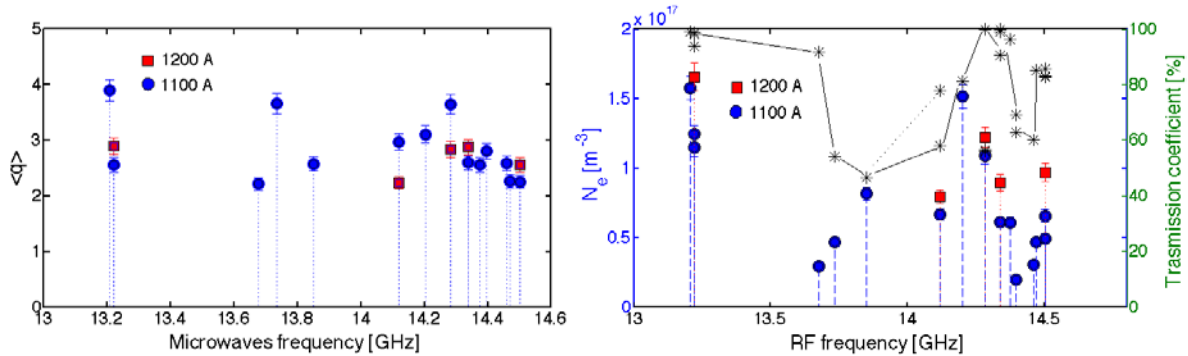
Evidently a clear enhancement of the ion currents of all these charge states is achieved when the microwave frequency is set to an optimized condition. This effect is increasingly pronounced for the higher charge states. Over the complete power range the current enhancement factor remains constant for a given charge state of  $\text{Ar}^{q+}$  ( $q = 8, 9, 11$ ). For  $\text{Ar}^{12+}$ , this enhancement factor even increases with rising power.

Under the same collaboration a new experiment was carried out at GSI concerning the detection of X-radiation produced by the CAPRICE ECRIS-plasma under different input frequencies. To investigate the impact of the electromagnetic field modal structure on the plasma spatial distribution, heating process, beam formation, current and charge states, The setups shown in figure 11 were designed and assembled. The energy-dispersive X-ray spectrometry was carried out by making use of two X-ray detectors operating in two different energy ranges when the source was operated at different microwave frequencies with an Ar plasma, and at two magnetic field profiles ( $B_{\text{inj}}=1$  T and  $B_{\text{ext}}$  equal to 1.2 T and 1.26 T).



**Figure 11:** *SETUP-1 (up): the SDD is placed beyond a 20mm thick - 1mm hole Pb collimator, in air. SETUP 2 (down): the HpGe detector placed after the bending magnet.*

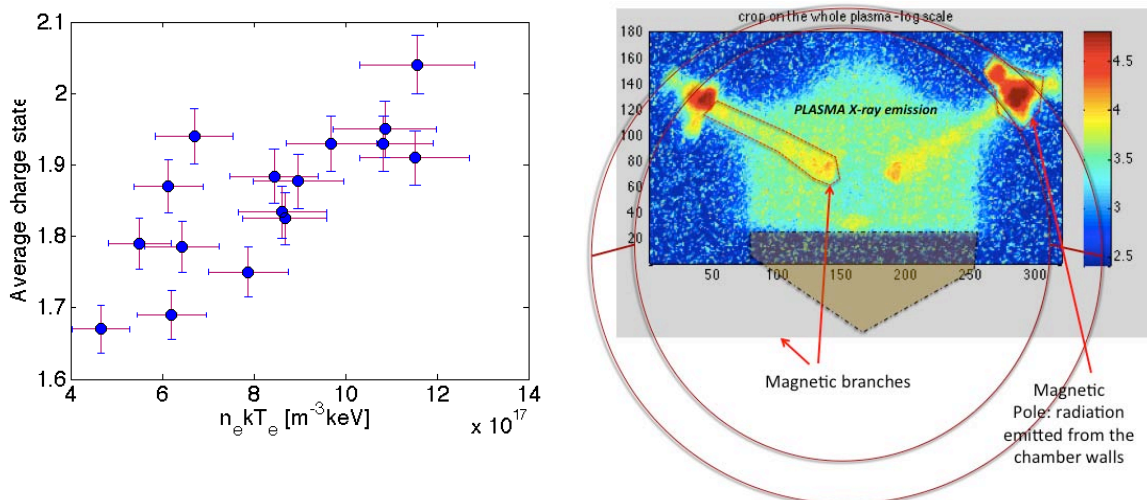
A plasma emissivity model was applied in order to extract density and temperature values. Figures 12 reassume the experimental results.  $\langle q \rangle$  varies in a non monotonical way with the pumping frequency. Fluctuations are relevant, even of a factor 2. Because of pressure variation, one-to-one correlation between density and  $\langle q \rangle$  at each frequency must be done with some caution, but nevertheless, these data are extremely interesting since for the first time a strong density fluctuation caused by the frequency tuning has been directly observed: the density fluctuates from around  $2 \cdot 10^{11} \text{ cm}^{-3}$  down to  $1.8 \cdot 10^{10} \text{ cm}^{-3}$ , i.e. more than one order of magnitude after few hundreds of MHz of frequency tuning. About the absolute values, considering that the density cutoff is around  $2.4 \cdot 10^{12} \text{ cm}^{-3}$  at 14 GHz, the concentration of warm electrons in the near axis region reaches a fraction  $>1-10\%$  of the total plasma density at the RF power supplied during the experiment, confirming relatively low density values as it comes out from simulations. While the density fluctuates of a factor 10, the temperature of a factor 2 at maximum. An increase of density (relevant) and temperature (less relevant) was observed when increasing the extraction field.



**Figure 12:** (left) Trend of  $\langle q \rangle$  versus the pumping wave frequency for the two different Bext field values. (right) Electron density extracted from SDD spectra versus RF frequency; the RF transmission coefficient is also shown in % on the right-hand side axis.

This field variation implies that the minimum B field is closer to the ECR level ( $B_0=0.3875$  T instead of 0.375 T). The plasmoid is slightly smaller but the gradient at ECR in the extraction side is slightly higher (few % of increase from 6.075 to 6.425 T/m). When varying the magnetic field, although the energy content  $N_e k T_e$  increases monotonically, not the same behaviour is observed for  $\langle q \rangle$ . In summary, the increased energy content is a necessary but not sufficient to establish better ionization conditions, as the ion confinement time also plays an important role. The latter result is explainable only on the basis of frequency tuning impact on ion dynamics.

A new setup based on a CCD camera coupled to a small pin-hole for X-ray imaging and space resolved spectroscopy has been designed, assembled and tested in November 2014 at ATOMKI – Debrecen (Hungary). As propaedeutic stage to CCD setu-up, SDD and HpGe detectors were used to formerly characterize the volumetric plasma emission, in a similar way to GSI experiment. As an important upgrade with respect to previous measurements, the SDD detector has been placed on the injection side of the ATOMKI ECRIS in order to allow X-ray measurements and beam extraction (including CSD determination) at the same time, thus providing a direct relationship between the CSD and the plasma spectrum.



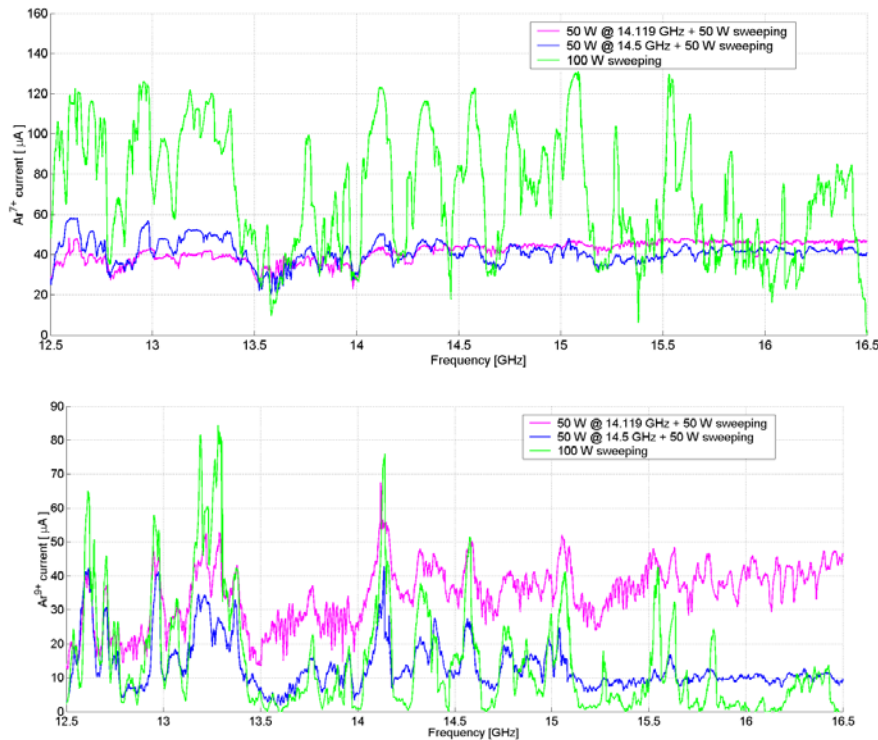
**Figure 13:** (left) average charge state as a function of the plasma energy content as measured by SDD spectra. Points refer to different RF frequency. (right) Imaging of the plasma obtained by the CCD camera pin-hole method.



Figure 13-left shows the trend of the  $\langle q \rangle$  as a function of plasma energy content. Each point corresponds to a different frequency, in the range 12.8-13.5 GHz, with steps of 40 MHz each.  $\langle q \rangle$  clearly grows with the energy content, but the scattered points demonstrate that it is not strictly a matter of density or temperature (or the product between them) being each  $\langle q \rangle$  obtainable by different combinations of energy contents, depending on the pumping wave frequency. We expect it is the shape of the plasma density, which plays a fundamental role, that gives the explanation to these data, and not only the global energy deposited into the warm electrons population, as detectable by the SDD. This motivated the X-ray imaging and space resolved spectroscopy (XSRS). Hereby we will show just imaging for a single excitation frequency (figure 13-right). Color scale refers to the number of photoelectrons produced in each pixel (therefore related to the flux of X-rays impinging on it). It is clearly visible the general structure of the plasma, the hole in the near axis region, the branches due to the electrons escaping from the confinement and the hot spots due to lost electrons producing bremsstrahlung radiation when impinging on the chamber walls. Several features of the plasma structure are already clear from this picture, providing a very positive feedback to the modeling efforts that will be presented later on. The consistent amount of collected data, along with their scientific relevance, will impose a detailed data analysis that will continue during the first months of 2015. Therefore we expect that this experiment will provide significant outputs even well beyond the expiration date of the ARES program.

#### 4. Double frequency measurements (GSI,LNS,IKF,IFIN-HH)

The technique of using feeding systems with two electromagnetic waves at different frequencies is called "double frequency heating" and hereinafter the results of applying this technique on the CAPRICE ion source at the GSI test-bench, in collaboration with the LNS team, are described. As reported above the effect of the frequency tuning on the ion current intensities is promising. The Ar charge state distributions were analysed for different frequencies and it has been reported that for some of them, i.e. 14.119 GHz, an enhanced intensity of the higher charge states occurred. The frequencies 14.119 and 14.5 GHz were selected as fixed frequencies to analyse the CAPRICE performances in terms of higher current and production of higher charge states when the second sweeping frequency, in the 12.5-16.5 GHz range, was applied. A power combiner was used to send to the TWTA two electromagnetic waves with different frequency provided by two sweeping generators. The output power from the TWTA was kept at 100 W (the output power of each generator was balanced). Then the  $\text{Ar}^{7+}$ ,  $\text{Ar}^{8+}$  and  $\text{Ar}^{9+}$  currents and the drain current were measured during the frequency sweep of the second signal generator. A more stable behaviour of the ion current with the frequency is observed in the evolution both of the  $\text{Ar}^{7+}$  and of the  $\text{Ar}^{9+}$  ion currents (figures 14). For the  $\text{Ar}^{9+}$  the average level of the ion current is higher with respect to the case of the single frequency tuning but for the frequencies when a current peak occurs the level is higher in the case of the single frequency tuning. With respect to the 14.5 GHz fixed frequency, at 14.119 GHz the higher charge states tend to higher ion currents when increasing the frequency. Then, when operating in the double frequency heating and when optimizing one of the two frequencies the current increases linearly with the second frequency.



**Figure 14:** Effect on the  $Ar^{7+}$  (up) and  $Ar^{9+}$  (down) current of the double frequency heating for two settings of the fixed frequency and comparison with the single frequency tuning.

#### 4 – MD method in the ECR plasma (IFIN-HH and IKF)

The MD method as a tool of investigation of the physical properties and processes of the ECR plasma has been continued and the influence of the extraction voltage on the high energy slope of Bremsstrahlung radiation spectra has been reported. This was the subject of a dedicated study at the IKF –ECRIS. Most of the new generation ECRIS installations use Double Frequency Heating (DFH) and Frequency Tuning (FT) to increase the very high charge states intensities.

We have carried out a series of dedicated experiments to study the influence of an enhanced EEDF, created by using the MD method, onto the performance of DFH. A MD liner turns the ECRIS into a higher performing source. Additionally it was observed that the efficiency of the gas mixing method, when plasma-wall interaction is significant, is reduced in our experiment to 35% versus the standard ECRIS gas mixing efficiency [RSI, 83, 2, 02A348, (2012)]. We have measured Bremsstrahlung radiation spectra by monitoring the  $Ar^{14+}$  charge state as the extraction voltage is changed from zero to 20 kV. In order to provide supplementary information, a 90 mm length MD liner was introduced in the plasma chamber covering the inner walls. The shape of the spectra are identical, however, the total yields for the MD configuration are in average three times lower (as expected for the configuration). The total X-ray yields (detected in the range 140-200 keV) monitored as a function of the extracted voltage confirm that the extraction voltage does not change the rate of x-rays. We can conclude that the Bremsstrahlung measurements did not put in evidence a change concerning the plasma energetic electron population. [RSI 83, 2, 02A331, (2012)]. In order to gain information on the DFH-mechanism and on the role of the lower injected frequency we have put emphasis on the creation of a discrete resonance surface also for this lower

frequency. Our established method of inserting an emissive MD (metal-dielectric) liner into the plasma chamber of the source is used in these experiments as a tool of investigation. In this way the electron temperature and density for both ECR zones is increased in a controlled manner, allowing conclusions on the role of the change of the EEDF with and without DFH.

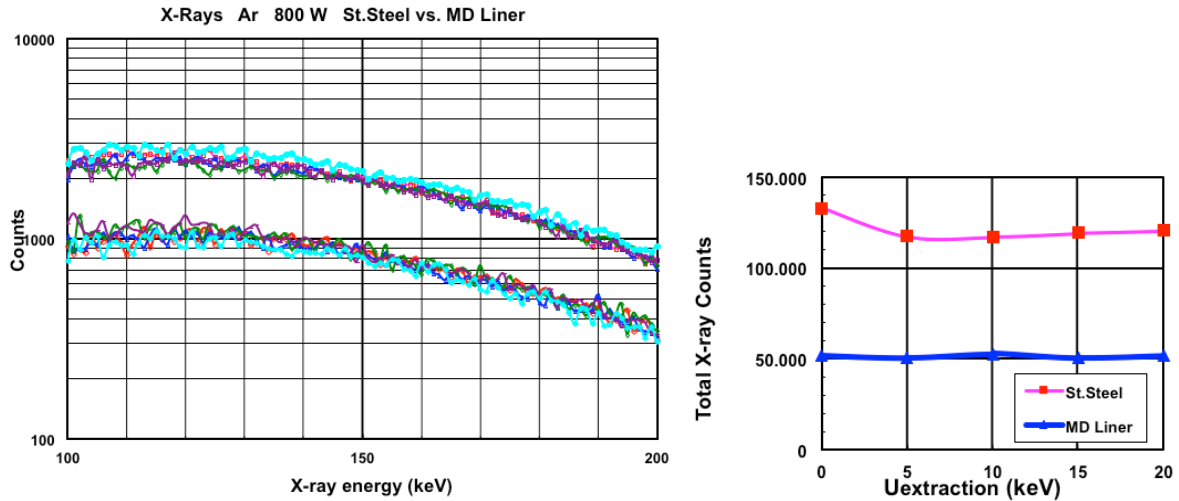


**Figure 15:** left – X -ray spectra in case of stainless steel or MD covered plasma chamber walls. Right – Total X-ray counts vs. extraction voltage in case of stainless steel or MD covered plasma chamber walls.

**PUBLICATIONS:**

## Peer Reviewed Articles:

- 1.1. J. Rubert, J. Piot, Z. Asfari, B.JP. Gall, J. Ärje, O. Dorvaux, P.T. Greenlees, H. Koivisto, A. Ouadi, R. Seppälä, First intense isotopic titanium-50 beam using MIVOC method, Nucl. Instrum. and Meth. in Phys. Res. B 276 (2012), p. 33.
- 1.2. I. Izotov, V. Skalyga, V. Zorin, O. Tarvainen, H. Koivisto, Plasma instability in the afterglow of ECR discharge sustained in a mirror trap, Physics of Plasmas, 19, (2012), p. 122501.
- 1.3. V. Toivanen, O. Tarvainen, J. Komppula and H. Koivisto, Oscillations of ECR ion source beam current along the beam transport of the JYFL K-130 cyclotron, Journal of Instrumentation (IOP Science), Vol. 8, (2013), T02005.
- 1.4. V. Toivanen, T. Kalvas, H. Koivisto, J. Komppula and O. Tarvainen, Double einzel lens extraction for the JYFL 14 GHz ECR ion source designed with IBSimu, J. Instrum. 8(2013) P05003.
- 1.5. V. Toivanen, O. Tarvainen, J. Komppula and H. Koivisto, The effect of plasma electrode collar structure on the performance of the JYFL 14 GHz electron cyclotron resonance ion source, Nucl. Instrum. Meth. A 726 (2013), p. 41–46.
- 1.6. O. Tarvainen, I. Izotov, D. Mansfeld, V. Skalyga, S. Golubev, T. Kalvas, H. Koivisto, J. Komppula, R. Kronholm, J. Laulainen and V. Toivanen, Beam current oscillations driven by cyclotron instabilities in a minimum-*B* electron cyclotron resonance ion source plasma, IOP-select: Plasma Sources Sci. Technol. 23 (2014), p. 025020.
- 1.7. D. Mascali, G. Torrioni, L. Neri, G. Sorbello, G. Castro, L. Celona, and S. Gammino. 3D-full wave and kinetics Numerical modelling of Electron Cyclotron Resonance Ion Sources plasma: steps towards self-consistency, accepted for publication on European Physical Journal – D.
- 1.8. D. Mascali, S. Gammino, L. Celona, G. Ciavola, *Towards a better comprehension of plasma formation and heating in high performance ECRIS - invited*, Rev. Sci. Instrum. 83, 02A336 (2012).
- 1.9. L. Neri, D. Mascali, L. Celona, S. Gammino, G. Ciavola, *A 3D MonteCarlo code for the modelling of plasma dynamics and beam formation mechanism in ECR ion sources*, Rev. Sci. Instrum. 83, 02A330 (2012);
- 1.10. D. Mascali, L. Neri, L. Celona, G. Castro, G. Torrioni, S. Gammino, G. Sorbello and G. Ciavola. A double-layer based model of ion confinement in ECRIS. Rev. Sci. Instrum. 85, 02A511 (2014); <http://dx.doi.org/10.1063/1.4860652>
- 1.11. D. Mascali, L. Celona, F. Maimone, J. Maeder, G. Castro, F.P. Romano, A. Musumarra, C. Altana, C. Caliri, G. Torrioni, L. Neri, S. Gammino, K. Tinschert, K. P. Spaedtke, J. Rossbach, R. Lang and G. Ciavola. *X-ray spectroscopy of warm and hot electron components in the CAPRICE source plasma at EIS testbench at GSI*. Rev. Sci. Instrum. 85, 02A956 (2014); <http://dx.doi.org/10.1063/1.4858115>
- 1.12. G. Castro, D. Mascali, P. Romano, L. Celona, S. Gammino, R. Di Giugno, D. Lanaia, R. Miracoli, T. Serafino and G. Ciavola, Comparison between off-resonance and E.B.W. heating regime in a Microwave Discharge Ion Source, Rev. Sci. Instrum. 83, 02B501 (2012).
- 1.13. L. Schachter, K. E. Stiebing and S. Dobrescu, The impact of plasma-wall interaction on the gas mixing efficiency in electron cyclotron resonance ion source, Rev. of Sci. Instrum., vol 83, 2, 02A 348, 2012
- 1.14. K. E. Stiebing, L. Schachter, and S. Dobrescu, The influence of the extraction voltage on the energetic electron population of an electron cyclotron resonance ion source plasma, , Rev. of Sci. Instrum., vol 83, 2, 02A 331, 2012
- 1.15. L. Schachter, K. E. Stiebing and S. Dobrescu, On the role of Electron Energy Distribution Function in Double Frequency Heating, Rev. of Sci. Instrum. 85, 02A919, 2014

## Peer Reviewed Conference Articles

- 2.1. O. Tarvainen, V. Toivanen, J. Komppula, T. Kalvas, J. Kauppinen and H. Koivisto, The effect of gas mixing and biased disc voltage on the preglow of ECRIS plasma, Rev. Sci. Instrum. 83, (2012), 02A314.
- 2.2. V. Toivanen, O. Tarvainen, J. Kauppinen, J. Komppula, and H. Koivisto, ECRIS plasma chamber studies using a network analyzer as a loaded cavity probe, Rev. Sci. Instrum. 83, 02A306 (2012).
- 2.3. J. Komppula, O. Tarvainen, S. Lätti, T. Kalvas, H. Koivisto, V. Toivanen and P. Myllyperkiö, VUV-diagnostics of a filament-driven arc discharge H<sup>+</sup> ion source, Third International Symposium on



- Negative Ions, Beams and Sources (NIBS 2012), 3-7 Sept. (2012), Jyväskylä, Finland, AIP Conference Proceedings 1515, (2013), p. 66.
- 2.4. T. Kalvas, O. Tarvainen, J. Komppula, M. Laitinen, T. Sajavaara, H. Koivisto, A. Jokinen, and M.P. Dehnel, Recent negative ion source activity at JYFL, Third International Symposium on Negative Ions, Beams and Sources (NIBS 2012), 3-7 Sept. (2012), Jyväskylä, Finland, AIP Conference Proceedings 1515, (2013), p. 349.
  - 2.5. Olli Tarvainen, Ville Toivanen, Jani Komppula, Taneli Kalvas, and Hannu Koivisto, Transverse Distribution of Beam Current Oscillations of a 14 GHz Electron Cyclotron Resonance Ion Source, *Rev. Sci. Instrum.* **85**, (2014), 02A909.
  - 2.6. H. Koivisto, O. Tarvainen, V. Toivanen, J. Komppula, R. Kronholm, T. Lamy, J. Angot, P. Delahaye, L. Maunoury, A. Galata, G. Patti, L. Standylo, O. Steczkiewicz and J. Choinski, Ionization Efficiency Studies with Charge Breeder and Conventional ECRIS *Rev. Sci. Instrum.* **85**, (2014), 02B917.
  - 2.7. T. Kalvas, O. Tarvainen, J. Komppula, H. Koivisto, D. Potkins, T. Stewart and M. P. Dehnel, A CW radiofrequency ion source for production of negative hydrogen ion beams for cyclotrons, Fourth International Symposium on Negative Ions, Beams and Sources (NIBS 2014), 6-10 Oct. (2014), Garching, Germany, Accepted for publication.
  - 2.8. J. Laulainen, T. Kalvas, H. Koivisto, J. Komppula and O. Tarvainen, Photoelectron emission from metal surfaces induced by VUV-emission of filament driven hydrogen arc discharge plasma, Fourth International Symposium on Negative Ions, Beams and Sources (NIBS 2014), 6-10 Oct. (2014), Garching, Germany, Accepted for publication.
  - 2.9. J. Komppula, T. Kalvas, H. Koivisto, J. Laulainen and O. Tarvainen, Experimental study of waveguide coupled microwave heating with conventional multicusp negative ion sources, Fourth International Symposium on Negative Ions, Beams and Sources (NIBS 2014), 6-10 Oct. (2014), Garching, Germany, Accepted for publication.

#### Not peer reviewed articles:

- 3.1. H. Koivisto, O. Tarvainen, V. Toivanen, T. Kalvas, J. Komppula, J. Ärje, J. Laulainen and R. Kronholm, ECRIS related research and development work at JYFL and some future prospects, (ECRIS12: JACOW), Sydney, Australia, FRYA03.
- 3.2. O. Tarvainen, H. Koivisto, J. Komppula, V. Toivanen, C. M. Lyneis, M. M. Strohmeier, An Experimental Study of ECRIS Plasma Stability and Oscillation of Beam Current, (ECRIS12: JACOW), Sydney, Australia, TUXO02.
- 3.3. V. Toivanen, T. Kalvas, H. Koivisto, J. Komppula, O. Tarvainen, New Extraction Design for the JYFL 14 GHz ECRIS, (ECRIS12: JACOW), Sydney, Australia, TUZO03.
- 3.4. I. Izotov, D. Mansfeld, V. Skalyga, V. Zorin, T. Grahn, T. Kalvas, H. Koivisto, J. Komppula, P. Peura, O. Tarvainen, V. Toivanen, Plasma Instability in the Afterglow of ECR Discharge Sustained in a Mirror Trap, (ECRIS12: JACOW), Sydney, Australia, WEPP03.
- 3.5. H. Koivisto, O. Tarvainen, T. Kalvas, K. Ranttila, P. heikkinen, D. Xie, G. Machicoane, T. Thuillier, V. Skalyga, I. Izotov, HIISI, new 18 GHz ECRIS for the JYFL accelerator laboratory, (ECRIS-2014: JACOW), Nizhny Novgorod, 24-28 Aug. 2014, Russia, will be published in JACOW website.
- 3.6. T. Kalvas, O. Tarvainen, H. Koivisto, K. Ranttila, Thermal design of refigerated hexapole 18 GHz ECRIS HIISI, (ECRIS-2014: JACOW), Nizhny Novgorod, 24-28 Aug. 2014, Russia, will be published in JACOW website.
- 3.7. K. E. Stiebing, L. Schachter and S. Dobrescu, Secondary-Electron-Enhanced Plasma as an Alternative to Double/Variable-Frequency Heating in ECRIS, Proceedings of ECRIS2012, Sydney, Australia (2012), TUYO03, <http://jacow.org/>